Clim. Past Discuss., 10, 4623–4646, 2014
www.clim-past-discuss.net/10/4623/2014/
doi:10.5194/cpd-10-4623-2014

Climate of the Past
Discussions
Open Access

Multiscale monsoon variability during the last two climatic cycles inferred from Chinese loess and speleothem records

Y. Li[1], N. Su[2,3], L. Liang[1], L. Ma[1], Y. Yan[1], and Y. Sun[1]

[1]State Key Laboratory of Loess and Quaternary Geology, Institute of Earth Environment, Chinese Academy of Sciences, Xi'an 710075, China
[2]College of Science, Technology and Engineering, James Cook University, Cairns, Queensland 4870, Australia
[3]School of Mathematics and System Science, Shenyang Normal University, Shenyang 110034, China

Received: 24 October 2014 – Accepted: 12 November 2014 – Published: 20 December 2014

Correspondence to: Y. Li (liying@ieecas.cn) and Y. Sun (sunyb@ieecas.cn)

Published by Copernicus Publications on behalf of the European Geosciences Union.

Multiscale monsoon variability during the last two climatic cycles

Y. Li et al.

Abstract

The East Asian Monsoon exhibits a significant variability on timescales ranging from tectonic to centennial as inferred from Chinese loess, stalagmite and marine records. However, the relative contributions and plausible driving forces of the signals at different timescales remain poorly investigated. Here, we spectrally decompose time series data on loess grain size and speleothem $\delta^{18}O$ records over the last two climatic cycles and correlate the decomposed components with possible driving parameters including the ice volume, insolation and North Atlantic cooling. Based on the spectral analysis of these two proxies, we tentatively identified six components of the signals corresponding to various forcing of ice volume (> 50 kyr), obliquity (50–30 kyr), precession (30–9 kyr), North Atlantic cooling (9–3 kyr and 3–1 kyr), and a centennial residual. The relative contributions of each component differ significantly between loess grain size and speleothem $\delta^{18}O$ records. Glacial and orbital components are dominant in the loess grain size, which implies that both ice volume and insolation have distinctive impacts on the winter monsoon variability in contrast to the predominant precession impact on the summer monsoon patterns. Moreover, the millennial components are evident with variances of 11 and 16 % in the loess grain size and speleothem $\delta^{18}O$ records, respectively. A comparison of the millennial-scale signals in these two proxies reveals that abrupt changes in the winter and summer monsoons over the last 260 kyr share common features and similar driving forces linked to high-latitude Northern Hemisphere climate.

1 Introduction

The East Asian Monsoon (EAM), as an integral part of Asian monsoon circulation, has played an important role in driving the East Asian palaeoenvironmental changes (An, 2000). The EAM fluctuations can be quantified as different time intervals, which range from thousands of years to intraseasonal periodicities, and the primary driving force of the monsoon variability on each timescale is not unique (An et al., 2015). Multiscale monsoon variability has been inferred from numerous proxies generated from deep-sea, eolian sediments, and speleothem records, which provide valuable insights into the changing processes and potential driving forces of the EAM variability (Wang et al., 1999, 2008; Yancheva et al., 2006; Sun et al., 2012). In particular, Chinese loess has been investigated intensively as a direct and complete preserver of the EAM changes (An et al., 1990; Liu and Ding, 1998; An, 2000) with great efforts on deciphering on the EAM variability at both orbital and millennial scales (Ding et al., 1994, 2002; Porter and An, 1995; Guo et al., 1996; Liu et al., 1999; Chen et al., 2006; Sun et al., 2012).

On the orbital timescale, the EAM variation recorded by Chinese loess-paleosol sequences is characterized by an alternation between the dry-cold winter monsoon and the wet-warm summer monsoon (Liu and Ding, 1998; An, 2000). A strong 100 kyr periodicity is detected in the Chinese loess particle size record, implying an important impact of glacial boundary conditions on the EAM evolution (Ding et al., 1995). Obliquity and precession signals are also clear in loess based proxies (Liu et al., 1999; Ding et al., 2002; Sun et al., 2006). Apart from these dominant periodicities, some harmonic periodicities related to orbital parameters are also found in the EAM records, which include the ~ 75, ~ 55, and ~ 30 kyr spectral peaks (Lu et al., 2003; Sun et al., 2006; Yang et al., 2011). In contrast, absolute-dated speleothem $\delta^{18}O$ records reveal a dominant 23 kyr cycle, implying a dominant role of the summer insolation in driving the summer monsoon variability (Wang et al., 2008; Cheng et al., 2009). Different variances of obliquity and precession signals in monsoonal proxies suggest that the responses of the winter and summer monsoons to orbital forcing are dissimilar (Shi et al., 2011). The various patterns of orbital-scale monsoon fluctuations between the loess magnetic susceptibility and speleothem $\delta^{18}O$ records likely reflect the sensitivity of various archives and proxies to the EAM variability (Clemens et al., 2010; Cheng et al., 2012).

At the millennial timescale, the rapid monsoon oscillations inferred from Chinese loess are not only persistent during the last two glacial cycles (Porter and An, 1995;

Guo et al., 1996; An and Porter, 1997; Chen et al., 1997; Ding et al., 1999; Sun et al., 2010; Yang et al., 2014), they are also evident during early glacial extreme climatic conditions (Lu et al., 1999). The millennial-scale monsoon variability during the last glacial period is strongly coupled to climate changes recorded in Greenland ice-core and North Atlantic sediments, indicating a dynamical connection between the EAM variability and the high-latitude Northern Hemisphere climate (Porter and An, 1995; Guo et al., 1996; Chen et al., 1997; Fang et al., 1999). Recently, a combination of proxies from Chinese loess, speleothem, and Greenland ice-core with modeling results indicates that the Atlantic meridional overturning circulation might have played an important role in driving the rapid monsoon changes in East Asia (Sun et al., 2012).

Though previous studies have revealed that past EAM variabilities principally comprise a mixture of forcing signals from ice volume, solar radiation, and North Atlantic climate, the relative contributions of glacial, orbital and millennial forcing to the EAM variability remain unclear. In this study, we apply the spectral analysis to investigate the EAM variability with the 260 kyr mean grain size (MGS) record from a Gulang loess sequence as a parameter of the East Asian winter monsoon variations over the last two glacial–interglacial cycles, and the speleothem δ^{18}O record of Hulu and Sanbao caves as indicator of the orbital-to-millennial East Asian summer monsoon variability (Wang et al., 2008; Cheng et al., 2009). These two representative time series were decomposed to obtain principle components of the climatic signals, which were further compared with potential driving factors. Our objectives are to evaluate the relative variances of glacial–interglacial to millennial variabilities registered in the EAM and to address their causal links to external and internal forcing.

2 Materials and methods

The data for the loess sequence was collected at a section in Gulang, Gansu Province, China (37.49° N, 102.88° E, 2400 m a.s.l.), which is situated in the northwestern part of the Chinese Loess Plateau. It is about 10 km to the southwest margin of the Tengger

CPD
10, 4623–4646, 2014

desert (Fig. 1). In this region, the average annual precipitation and temperature over the last 20 years are 352 mm and 5.7 °C, respectively. About 70 m loess was accumulated at Gulang during the last two climate cycles. High sedimentation rate and weak pedogenesis in this region make the Gulang loess sequence very sensitive to rapid monsoon changes (Sun et al., 2012). The samples used in this study were collected at the Gulang section using 2 cm intervals, corresponding to 50–100 yr resolution for the loess-paleosol sequence. Before the measurements of grain sizes, all samples were firstly pretreated by removing carbonate and organic matter using 30 % HCl and 10 % H_2O_2, respectively, and then dispersed under ultrasonification in 10 mL 10 % $(NaPO_3)_6$ solution. A Malvern 2000 laser instrument was employed for determining the grain size distribution which has an analytical error of < 2 % as revealed by replicate analyses.

The chronology of the Gulang loess-paleosol sequence was generated using a weighted grain size model (Porter and An, 1995; Hao et al., 2012). Tie points for the age construction were determined by correlating rapid MGS changes to the terminations in benthic δ^{18}O (Lisiecki and Raymo, 2005) and absolute-dated speleothem δ^{18}O records (Wang et al., 2008; Cheng et al., 2009) (Fig. 2). Consistent with previous correlations between Chinese loess and deep-sea oxygen isotope records (Bloemendal et al., 1995; Ding et al., 1995, 2001, 2002; Liu et al., 1999), we correlate the transitions of S_0/L_1, L_1/S_1, S_1/L_2, L_2/S_2, and S_2/L_3 to the boundaries of marine isotope stages (MIS) 1/2 (13.2), 4/5 (76), 5/6 (130), 6/7 (190), and 7/8 (244 kyr), respectively (Fig. 2). In addition, the rapid loess MGS variation can be well correlated to abrupt changes in speleothem δ^{18}O record at 27, 38, 50, 60, 112, 166 and 228 kyr, respectively. All together, twelve tie points are selected for the age construction and sediment rate estimation (Fig. 2). Due to the coeval changes between sedimentation rate and grain size (Ding et al., 2001), the chronology between the tie points can be estimated using the weighted grain-size model proposed by Porter and An (1995).

As the widely used proxy for changes in the intensity of the summer monsoon, the absolute-dated speleothem δ^{18}O records from Sanbao and Hulu caves (Fig. 1) are selected for the duration of the last two glacial–interglacial cycles (Wang et al., 2008;

CPD
10, 4623–4646, 2014

Cheng et al., 2009) to compare fluctuations of each component at various timescales with loess grain size. For multiscale climatic research, spectral analysis is a primary tool to separate the variance of a time series into different principle components. We perform a spectral analysis on the 260 kyr records of Gulang MGS and speleothem $\delta^{18}O$ using REDFIT software (Schulz and Mudelsee, 2002). The decomposed components of loess MGS and speleothem $\delta^{18}O$ records are separated out using a filtering approach (Origin 8.0, OriginLab Corporation, USA) based on the spectrum results.

3 Multiscale monsoon variability

The spectral analysis shows that apparent periods identified in the MGS spectrum are at ~ 100, ~ 41, ~ 23, ~ 15, ~ 7.5, ~ 5.1–3.7, ~ 2 and ~ 1.3 kyr, respectively, over the 80 % confidence level (Fig. 3). It is shown that the potential forcing of the glacial–interglacial and orbital EAM variability is part of the external (e.g., the orbital-induced summer insolation, An et al., 1991; Wang et al., 2008) and the internal factors (e.g., changes in ice volume and CO_2 concentrations, Ding et al., 1995; Lu et al., 2013). The co-existence of the ~ 100, ~ 41, and ~ 23 kyr periods in the Gulang MGS record confirms the dynamical linkage of the winter monsoon variability to glacial and orbital forcing. For this reason, the components of global ice volume, obliquity, and precession, referred to as C1 (> 50 kyr), C2 (50–30 kyr), and C3 (30–9 kyr), respectively, are separated (Fig. 3).

After removing C1, C2, and C3 from the initial MGS record, the remaining component primarily contains millennial-to-centennial signals. Based on the spectral results, the millennial frequencies can be further divided into two components: C4 (9–3 kyr) and C5 (3–1 kyr), which, possibly correspond, respectively, to the Heinrich (~ 6 kyr) rhythm and the Dansgaard–Oeschger (DO, ~ 1.5 kyr) cycles recorded in the North Atlantic sediments and Greenland ice core (Bond et al., 1993; Dansgaard et al., 1993; Heinrich et al., 1988). Taking into account the sampling resolution and surface mixing effect

CPD
10, 4623–4646, 2014

at Gulang, the residual component (< 1 kyr) might contain both centennial and noisy signals, which is excluded for further discussion.

Compared to the MGS spectral results based on the MGS data, the speleothem $\delta^{18}O$ spectrum shares similar peaks at the precession (~ 23 kyr) and millennial bands (~ 5, ~ 4.2, ~ 3.7, ~ 2.4, ~ 2, ~ 1.5, ~ 1.3, and ~ 1 kyr), but is lack of distinct peaks at ~ 100 kyr and ~ 41 kyr (Fig. 3) as neither of these two peaks reaches the 80 % confidence level. Notably, precession peaks at ~ 23 and ~ 19 kyr are more dominant in the speleothem $\delta^{18}O$ than in the loess MGS record. Moreover, the speleothem spectrum shows a peak over the 80 % confidence level centered at ~ 10 kyr frequency, which is, approximately, related to the semi-precession frequency. Although uncertainties exist in matching some spectral peaks between these two proxies, the overall correlativity between the spectra of Gulang MGS and speleothem $\delta^{18}O$ records is unambiguous from the precessional to millennial scales (Fig. 3). Thus, the speleothem $\delta^{18}O$ variability is also decomposed into six components identical to those of Gulang MGS results.

The six components of loess MGS and speleothem $\delta^{18}O$ records are separated out as presented in Fig. 4. The variability of Gulang MGS is dominated by glacial component (C1) with a variance of 41 %. Two orbital components (C2 and C3) contribute 18 and 28 % to the total variance, respectively. The variances of two millennial components (C4 and C5) are very close (5 ~ 6 %) in the Gulang MGS record while the residual centennial variance is about 2 %. By contrast, glacial (C1) and obliquity (C2) components are not clear in the speleothem $\delta^{18}O$ record with variances of 14 and 9 %, respectively. The precession component (C3), however, is the most dominant signal among the six components, accounting for nearly 59 % of the variance. The two millennial components are also evident with variances of 11 and 5 %, respectively, with the variance of the residual component being only about 1 %.

In addition to the differences in the variance, the amplitudes of the signals do not match as it can be seen in the six components in Fig. 4. For the loess MGS record, the signals clearly peak at ~ 100 and ~ 200 kyr in C1 component, and at about ~ 10, ~ 50, ~ 90, ~ 130, ~ 170, ~ 210, and ~ 250 kyr in C2 component with undoubted cycles at

CPD
10, 4623–4646, 2014

~ 100 kyr and ~ 40 kyr, respectively. These peaks, however, are not well represented in the filtered components of the speleothem $\delta^{18}O$ records, particularly for the C1 component. While both loess MGS and speleothem $\delta^{18}O$ records demonstrate obvious ~ 20 kyr cycles, the amplitude of the precessional variability is more significant in the speleothem $\delta^{18}O$ record and the phase relationship is variable between these two records. The variability of the C4 component is larger in the speleothem $\delta^{18}O$ record relative to that in the loess MGS record whereas the amplitudes of the C5 component are similar between these two records.

4 Dynamics of multiscale EAM variability

4.1 Glacial and orbital forcing of the EAM variability

We combine glacial (C1), obliquity (C2), and precession (C3) components of Gulang MGS record as a low-frequency signal (> 9 kyr) to reveal the glacial- and orbital-scale variations of the winter monsoon. The combination of C1 to C3 components of the speleothem $\delta^{18}O$ record is tentatively taken as an indicator of the summer monsoon variations on the same timescale. The glacial-to-orbital variations of the loess and speleothem records represent the total variances of ~ 87 and ~ 82 %, respectively. The low-frequency signals of the loess MGS and speleothem $\delta^{18}O$ records are compared to changes in the ice volume and solar insolation at 65° N to ascertain the plausible impacts of glacial and orbital factors on the EAM variability (Fig. 5).

The low-frequency component of the Gulang MGS record is well correlated with ice volume change inferred from the benthic $\delta^{18}O$ record (Lisiecki and Raymo, 2005), reinforcing the strong coupling between the winter monsoon variation and ice-volume changes (Ding et al., 1995). Besides the glacial–interglacial contrast, some fining MGS signals at the precessional scale are more distinctive than those of the benthic $\delta^{18}O$ stack. For example, the abrupt decrease in the MGS around 55, 80, 110, and 170 kyr have no counterpoints in the benthic $\delta^{18}O$ record. By comparing MGS data with the summer insolation record, the overall ~ 20 kyr periodicity is shown to be visible during winter monsoons with variable amplitudes (Fig. 5). These changes, however, present no remarkable fining of the loess MGS corresponds to the strong solar insolation around 150 and 220 kyr. Nevertheless, the coexistence of the glacial and orbital cycles in loess MGS indicates that both the ice volume and solar insolation have affected the winter monsoon variability, and their relative contributions are almost equivalent as estimated from variances of the glacial and orbital components.

The speleothem $\delta^{18}O$ record varies quite synchronously with the July insolation, characterized by a dominant precession frequency (Fig. 5). This in-phase change is thought to support a dominant role of summer insolation in Northern Hemisphere in driving the summer monsoon variability at the precession period (Wang et al., 2008), given that the paleoclimatic interpretation of the speleothem $\delta^{18}O$ is quite controversial (Wang et al., 2001, 2008; Yuan et al., 2004; Hu et al., 2008; Cheng et al., 2009; Peterse et al., 2011). The different transitions from the glacial to the orbital variability between the loess MGS and speleothem $\delta^{18}O$ records indicate that the forcing associated with these two proxies is different. The loess grain size is directly related to the northwesterly wind intensity, reflecting atmospheric surface processes is linked to the Siberian-Mongolian High (Porter and An, 1995), whereas the speleothem $\delta^{18}O$ might be influenced by multiple factors such as the isotopic depletion along the vapor transport path (Pausata et al., 2011), changes in $\delta^{18}O$ values of meteoric precipitation or the amount of summer monsoon precipitation (Wang et al., 2001, 2008; Cheng et al., 2009), and seasonality in the amount and isotopic composition of rainfall (Clemens et al., 2010; Dayem et al., 2010; Maher and Thompson, 2012).

It is quite clear that the EAM is formed by the thermal gradient between the Asian continent and the Pacific Ocean to the east and southeast (Halley, 1986; Xiao et al., 1995; Lestari and Iwasaki, 2006). In winter, due to a much larger heat capacity of water in the ocean than that on the land surface, a higher barometric pressure forms over the colder Asian continent with a lower pressure over the warmer ocean. This gradient is the driving forces for the flow of cold and dry air out of Asia, consequently, the winter

CPD
10, 4623–4646, 2014

monsoon forms (Gao, 1962). On the glacial–interglacial timescale, the buildup of the northern high-latitude ice sheets during the glacial periods strengthens the barometric gradient which results in intense winter monsoons (Ding et al., 1995; Clark et al., 1999). The contemporaneous falling sea level further enhances the winter monsoon circulation because of a larger distance between the land and the ocean, therefore a greater pressure gradient forms (Xiao et al., 1995). The other factor that influences the land-ocean differential thermal motion is the changes due to the orbitally induced solar radiation. The precession-induced insolation changes can lead to regional land-ocean thermal gradients whilst obliquity-related insolation changes can result in meridional thermal gradients; both of which can substantially alter the evolution of the Siberian and Subtropical Highs and the EAM variations (Shi et al., 2011).

4.2 Impacts of high-latitude cooling on millennial EAM oscillations

The EAM variations are proved to generally follow the combined influences of the induced global ice volume and Northern Hemisphere summer insolation and are persistently punctuated by apparent millennial-scale monsoon events (Garidel-Thoron et al., 2001; Wang et al., 2001; Kelly et al., 2006). The millennial-scale events of the last glacial cycle were firstly identified in Greenland ice cores (Dansgaard et al., 1993; Meese et al., 1997). Subsequently, well-dated loess grain size and speleothem δ^{18}O records in China have been found to have apparent correspondences with rapid climate oscillations in the North Atlantic (Porter and An, 1995; Guo et al., 1996; Chen et al., 1997; Ding et al., 1998; Wang et al., 2001). The most striking evidence is the strong correlation between the loess grain size, speleothem δ^{18}O and Greenland ice-core δ^{18}O records during the last glaciation (Ding et al., 1998; Wang et al., 2001; Sun et al., 2012). These abrupt changes have been extended into the last three glacial–interglacial cycles from loess and speleothem records (Ding et al., 1999; Cheng et al., 2006, 2009; Wang et al., 2008; Yang and Ding, 2014) and from the North Atlantic sediments (McManus et al., 1999; Channell et al., 2012).

CPD
10, 4623–4646, 2014

Here C4 and C5 components of the loess MGS and speleothem $\delta^{18}O$ records can be considered as millennial-scale signals of the winter and summer monsoons, with variances of 11 and 16 %, respectively. The combination of the two millennial signals of the loess MGS and speleothem $\delta^{18}O$ records are compared with the North Atlantic cooling events over the last two glacial cycles, to reveal the dynamical links of abrupt climate changes in East Asia and North Atlantic (Fig. 6). The Younger Dryas (YD) and Heinrich Events (H_1-H_6) are well detected in loess and speleothem records around 12, 16, 24, 31, 39, 48, 55, and 60 kyr, respectively, although the amplitude of coarsening MGS around 31 kyr seems to be weaker relative to H_3 event. Similarly, most of millennial-scale events in these two records are well aligned with comparable amplitude and duration during the last two glacial cycles. However, some MGS valleys such as A17, A24, B10, and B15–17 are not well matched with the speleothem $\delta^{18}O$ minima, possibly due to uncertainties in the loess chronology.

The millennial-scale monsoon signals have been well compared with the cooling events recorded in the North Atlantic sediments, demonstrating dynamical link between abrupt climate changes in East Asia and North Atlantic. As identified in Chinese speleothem records, the magnitudes of abrupt climate events are identical between the last and the penultimate climatic cycles (Wang et al., 2008). However, the duration and amplitude of these millennial events seems quite different between the glacials and interglacials. The duration of millennial monsoon events is relatively shorter and the amplitude larger during glacial periods, suggesting a plausible glacial modulation on rapid climate changes (McManus et al., 1999; Wang et al., 2008). The potential driving mechanism for rapid EAM changes has been attributed to changing climate in the high-latitude Northern Hemisphere, e.g., the reduction of the North Atlantic deep water circulation triggered by fresh water inputs from melting icebergs (Broecker, 1994). The North Atlantic cooling can affect the zonal high pressure systems, including Azores-Ural-Siberian-Mongolian high (Palmer and Sun, 1985; Rodwell et al., 1999; Yuan et al., 2004), which can further transmit the abrupt cooling effect into East Asian and result in significant EAM changes (Porter and An, 1995; Wang et al., 2001). Apart from

CPD
10, 4623–4646, 2014

the geological evidence, numerical modeling also suggests that the Atlantic meridional overturning circulation might affect abrupt oscillations of the EAM, while westerly jet is the important conveyor introducing the North Atlantic signal into the EAM region (Miao et al., 2004; Zhang and Delworth, 2005; Jin et al., 2007; Sun et al., 2012).

5 Conclusions

The orbital and millennial signals are spectrally decomposed from Chinese loess and speleothem records over the last two climatic cycles, permitting an evaluation of the relative contributions of orbital and millennial signals in the EAM record. Based on the amplitude variances, equivalent glacial and orbital impacts on the variation in loess grain size and a dominant precession forcing in the speleothem δ^{18}O variability are found. The millennial components are evident in the loess and speleothem proxies with variance of 11 and 16 %, respectively. The glacial–interglacial cycles play an important role in driving the winter monsoon fluctuations, which is in pace with the remarkable precession cycles in the speleothem δ^{18}O record. Different patterns of the periodicities and amplitude variances on the glacial- and orbital-scale variations between the loess and speleothem records might attribute either to a complicated relationship of these two proxies with the monsoonal wind strength and precipitation changes, or to distinctive responses of the winter and summer monsoons to the glacial and orbital forcing. There is a similarity of millennial-scale monsoon events both in terms of the magnitudes and rhythms, implying that the winter and summer monsoons share the common millennial features and similar driving force.

Acknowledgements. We thank J. Zhao, L. He, M. Zhao, and H. Wang for assistance in field sampling and lab measurements. This work was supported by funds from the National Basic Research Program of China (2013CB955904), the Chinese Academy of Sciences (KZZD-EW-TZ-03), the National Science Foundation of China (41 472 163), and the State Key Laboratory of Loess and Quaternary Geology (SKLLQG1011).

CPD
10, 4623–4646, 2014

References

An, Z.: Magnetic susceptibility evidence of monsoon variation on the Loess Plateau of central China during the last 130,000 years, Quaternary Res., 36, 29–36, 1991.

An, Z.: The history and variability of the East Asian paleomonsoon climate, Quaternary Sci. Rev., 19, 171–187, 2000.

An, Z. and Porter, S. C.: Millennial-scale climatic oscillations during the last interglaciation in central China, Geology, 25, 603–606, 1997.

An, Z., Liu, T., Lu, Y., Porter, S. C., Kukla, G., Wu, X., and Hua, Y.: The long-term paleomonsoon variation recorded by the loess-paleosol sequence in Central China, Quatern. Int., 7, 91–95, 1990.

An, Z., Wu, G., Li, J., Sun, Y., Liu, Y., Zhou, W., Cai, Y., Duan, A., Li, L., Mao, J., Cheng, H., Shi, Z., Tan, L., Yan, H., Ao, H., Chang, H., and Juan, F.: Global monsoon dynamics and climate change, Annu. Rev. Earth. Planet. Sci., 43, doi:10.1146/annurev-earth-060313-054623, 2015.

Bloemendal, J., Liu, X., and Rolph, T. C.: Correlation of the magnetic susceptibility stratigraphy of Chinese loess and the marine oxygen isotope record: chronological and palaeoclimatic implications, Earth Planet. Sc. Lett., 131, 371–380, 1995.

Bond, G., Broecker, W., Johnsen, S., McManus, J., Labeyrie, L., Jouzel, J., and Bonani, G.: Correlations between climate records from North Atlantic sediments and Greenland ice, Nature, 365, 143–147, 1993.

Broecker, W. S.: Massive iceberg discharges as triggers for global climate change, Nature, 372, 421–424, 1994.

Channell, J. E. T., Hodell, D. A., Romero, O., hillaire-Marcel, C., Vernal, A. D., Stoner, J. S., Mazaud, A., and Röhl, U.: A 750-kyr detrital-layer stratigraphy for the North Atlantic (IODP Sites U1302–U1303, Orphan Knoll, Labrador Sea), Earth Planet. Sc. Lett., 317–318, 218–230, 2012.

Chen, F., Bloemendal, J., Wang, J., Li, J., and Oldfield, F.: High-resolution multi-proxy climate records from Chinese loess: evidence for rapid climatic changes over the last 75 kyr, Palaeogeogr. Palaeocl., 130, 323–335, 1997.

Chen, J., Chen, Y., Liu, L., Ji, J., Balsam, W., Sun, Y., and Lu, H.: Zr/Rb ratio in the Chinese loess sequences and its implication for changes in the East Asian winter monsoon strength, Geochim. Cosmochim. Ac., 70, 1471–1482, 2006.

Cheng, H., Edwards, R. L., Kong, X., Ming, Y., Kelly, M. J., Wang, X., Gallup, C. D., and Liu, W.: A penultimate glacial monsoon record from Hulu Cave and two-phase glacial terminations, Geology, 34, 217–220, 2006.

Cheng, H., Edwards, R. L., Broecker, W. S., Denton, G. H., Kong, X., Wang, Y., Zhang, R., and Wang, X.: Ice age terminations, Science, 326, 248–252, 2009.

Cheng, H., Zhang, P., Spötl, C., Edwards, R. L., Cai, Y., Zhang, D., and Sang, W.: The climate cyclicity in semiarid-arid central Asia over the past 500,000 years, Geophys. Res. Lett., 39, L01705, doi:10.1029/2011GL050202, 2012.

Clark, P. U., Alley, R. B., and Pollard, D.: Northern Hemisphere ice-sheet influences on global climate change, Science, 286, 1104–1111, 1999.

Clemens, S. C., Prell, W. L., and Sun, Y.: Orbital-scale timing and mechanisms driving Late Pleistocene Indo-Asian summer monsoons: reinterpreting cave speleothem δ^{18}O, Paleoceanography, 25, PA4207, doi:10.1029/2010PA001926, 2010.

Dansgaard, W., Johnsen, S. J., Clausen, H. B., Dahl-Jensen, D., Gundestrup, N. S., Hammer, C. U., Hvidberg, C. S., Steffensen, J. P., Sveinbjornsdottir, A. E., Jouzel, J., and Bond, G.: Evidence for general instability of past climate from a 250-kyr ice-core record, Nature, 364, 218–220, 1993.

Dayem, K. E., Molnar, P., Battisti, D. S., and Roe, G. H.: Lessons learned from oxygen isotopes in modern precipitation applied to interpretation of speleothem records of paleoclimate from eastern Asia, Earth Planet. Sc. Lett., 295, 219–230, 2010.

Ding, Z., Yu, Z., Rutter, N. W., and Liu, T.: Towards an orbital time scale for Chinese loess deposits, Quaternary Sci. Rev., 13, 39–70, 1994.

Ding, Z., Liu, T., Rutter, N. W., Yu, Z., Guo, Z., and Zhu, R.: Ice-Volume forcing of East Asian winter monsoon variations in the past 800,000 years, Quaternary Res., 44, 149–159, 1995.

Ding, Z., Rutter, N. W., Liu, T., Ren, J., Sun, J., and Xiong, S.: Correlation of Dansgaard–Oeschger cycles between Greenland ice and Chinese loess, Paleoclimates, 4, 281–291, 1998.

Ding, Z., Ren, J., Yang, S., and Liu, T.: Climate instability during the penultimate glaciation: evidence from two high-resolution loess records, China, J. Geophys. Res., 104, 20123–20132, 1999.

Ding, Z., Yu, Z., Yang, S., Sun, J., Xiong, S., and Liu, T.: Coeval changes in grain size and sedimentation rate of eolian loess, the Chinese Loess Plateau, Geophys. Res. Lett., 28, 2097–2100, 2001.

CPD
10, 4623–4646, 2014

Ding, Z., Derbyshire, E., Yang, S., Yu, Z., Xiong, S., and Liu, T.: Stacked 2.6-Ma grain size record from the Chinese loess based on five sections and correlation with the deep-sea δ^{18}O record, Paleoceanography, 17, 5-1–5-21, 2002.

Fang, X., Pan, B., Guan, D., Li, J., Yugo, O., Hitoshi, F., and Keiichi, O.: A 60000-year loess-paleosol record of millennial-scale summer monsoon instability from Lanzhou, China, Chinese Sci. Bull., 44, 2264–2267, 1999.

Gao, Y.: On some problems of Asian monsoon, in: Some Questions About the East Asian Monsoon, edited by: Gao, Y., Science Press, Beijing, 1–49, 1962.

Garidel-Thoron, T. D., Beaufort, L., Linsley, B. K., and Dannenmann, S.: Millennial-scale dynamics of the East Asian winter monsoon during the last 200,000 years, Paleoceanography, 16, 491–502, 2001.

Guo, Z., Liu, T., Guiot, J., Wu, N., Lv, H., Han, J., Liu, J., and Gu, Z.: High frequency pulses of East Asian monsoon climate in the last two glaciations: link with the North Atlantic, Clim. Dynam., 12, 701–709, 1996.

Halley, E.: An historical account of the trade winds and monsoons observable in the seas between and near the tropics with an attempt to assign the physical cause of the said wind, Philos. T. R. Soc. Lond., 16, 153–168, 1986.

Hao, Q., Wang, L., Oldfeild, F., Peng, S., Qin, L., Song, Y., Xu, B., Qiao, Y., Bloemendal, J., and Guo, Z.: Delayed build-up of Arctic ice sheets during 400,000-year minima in insolation variability, Nature, 490, 393–396, 2012.

Heinrich, H.: Origin and consequences of cyclic ice rafting in the Northeast Atlantic Ocean during the past 130,000 years, Quaternary Res., 29, 142–152, 1988.

Hu, C., Henderson, G. M., Huang, J., Xie, S., Sun, Y., and Johnson, K. R.: Quantification of Holocene Asian monsoon rainfall from spatially separated cave records, Earth Planet. Sc. Lett., 266, 221–232, 2008.

Jin, L., Chen, F., Ganopolski, A., and Claussen, M.: Response of East Asian climate to Dansgaard/Oeschger and Heinrich events in a coupled model of intermediate complexity, J. Geophys. Res., 112, D06117,doi:10.1029/2006JD007316, 2007.

Kelly, M. J., Edwards, R. L., Cheng, H., Yuan, D., Cai, Y., Zhang, M., Lin, Y., and An, Z.: High resolution characterization of the Asian Monsoon between 146,000 and 99,000 years B. P. from Dongge Cave and global correlation of events surrounding Termination II, Palaeogeogr. Palaeocl., 236, 20–38, 2006.

CPD
10, 4623–4646, 2014

Lestari, R. and Iwasaki, T.: A GCM study on the roles of the seasonal marches of the SST and land–sea thermal contrast in the onset of the Asian summer monsoon, J. Meteorol. Soc. Jpn., 84, 69–83, 2006.
Lisiecki, L. E. and Raymo, M. E.: A Pliocene-Pleistocene stack of 57 globally distributed benthic δ^{18}O records, Paleoceanography, 20, PA1003, doi:10.1029/2004PA001071, 2005.
Liu, T. and Ding, Z.: Chinese loess and the paleomonsoon, Annu. Rev. Earth Pl. Sc., 26, 111–145, 1998.
Liu, T., Ding, Z., and Rutter, N.: Comparison of Milankovitch periods between continental loess and deep sea records over the last 2.5 Ma, Quaternary Sci. Rev., 18, 1205–1212, 1999.
Lu, H., Huissteden, K. V., An, Z., Nugteren, G., and Vandenberghe, J.: East Asia winter monsoon variations on a millennial time-scale before the last glacial–interglacial cycle, J. Quaternary Sci., 14, 101–110, 1999.
Lu, H., Zhang, F., and Liu, X.: Patterns and frequencies of the East Asian winter monsoon variations during the past million years revealed by wavelet and spectral analyses, Global Planet. Change, 35, 67–74, 2003.
Lu, H., Yi, S., Liu, Z., Mason, J. A., Jiang, D., Cheng, J., Stevens, T., Xu, Z., Zhang, E., Jin, L., Zhang, Z., Guo, Z., Wang, Y., and Otto-Bliesner, B.: Variation of East Asian monsoon precipitation during the past 21 k.y., and potential CO_2 forcing, Geology, 41, 1023–1026, 2013.
Maher, B. A. and Thompson, R.: Oxygen isotopes from Chinese caves: records not of monsoon rainfall but of circulation regime, J. Quaternary Sci., 27, 615–624, 2012.
McManus, J. F., Oppo, D. W., and Cullen, J. L.: A 0.5-million-year record of millennial-scale climate variability in the North Atlantic, Science, 283, 971–975, 1999.
Meese, D. A., Gow, A. J., Alley, R. B., Zielinski, G. A., Grootes, P. M., Ram, M., Taylor, K. C., Mayewski, P. A., and Blozan, J. F.: The Greenland Ice Sheet Project 2 depth-age scale: methods and results, J. Geophys. Res., 102, 26411–26423, 1997.
Miao, X., Sun, Y., Lu, H., Mason, J. A.: Spatial pattern of grain size in the Late Pliocene “Red Clay” deposits (North China) indicates transport by low-level northerly winds, Palaeogeogr. Palaeocl., 206, 149–155, 2004.
Palmer, T. N. and Sun, Z.: A modelling and observational study of the relationship between sea surface temperature in the North-West atlantic and the atmospheric general circulation, Q. J. Roy. Meteor. Soc., 111, 947–975, 1985.

CPD
10, 4623–4646, 2014

Multiscale monsoon variability during the last two climatic cycles

Y. Li et al.

Title Page
Abstract | Introduction
Conclusions | References
Tables | Figures
◂◂ | ▸▸
◂ | ▸
Back | Close
Full Screen / Esc
Printer-friendly Version
Interactive Discussion

Pausata, F. S. R., Battisti, D. S., Nisancioglu, K. H., and Bitz, C. M.: Chinese stalagmite $\delta^{18}O$ controlled by changes in the Indian monsoon during a simulated Heinrich event, Nat. Geosci., 4, 474–480, 2011.

Peterse, F., Prins, M. A., Beets, C. J., Troelstra, S. R., Zheng, H., Gu, Z., Schouten. S., Damsté, J. S. S.: Decoupled warming and monsoon precipitation in East Asia over the last deglaciation, Earth Planet. Sc. Lett., 301, 256–264, 2011.

Porter, S. C. and An, Z.: Correlation between climate events in the North Atlantic and China during the last glaciation, Nature, 375, 305–308, 1995.

Rodwell, M. J., Rowell, D. P., and Folland, C. K.: Oceanic forcing of the wintertime North Atlantic Oscillation and European climate, Nature, 398, 320–323, 1999.

Schulz, M. and Mudelsee, M.: REDFIT: estimating red-noise spectra directly from unevenly spaced paleoclimatic time series, Comput. Geosci., 28, 421–426, 2002.

Shi, Z. G., Liu, X. D., Sun, Y. B., An, Z. S., Liu, Z., and Kutzbach, J.: Distinct responses of East Asian summer and winter monsoons to astronomical forcing, Clim. Past, 7, 1363–1370, doi:10.5194/cp-7-1363-2011, 2011.

Sun, Y., Clemens, S. C., An, Z., and Yu, Z.: Astronomical timescale and palaeoclimatic implication of stacked 3.6-Myr monsoon records from the Chinese Loess Plateau, Quaternary Sci. Rev., 25, 33–48, 2006.

Sun, Y., Wang, X., Liu, Q., and Clemens, S. C.: Impacts of post-depositional processes on rapid monsoon signals recorded by the last glacial loess deposits of northern China, Earth Planet. Sc. Lett., 289, 171–179, 2010.

Sun, Y., Clemens, S. C., Morrill, C., Lin, X., Wang, X., and An, Z.: Influence of Atlantic meridional overturning circulation on the East Asian winter monsoon, Nature, 5, 46–49, 2012.

Wang, L., Sarnthein, M., Erlenkeuser, H., Grimalt, J., Grootes, P., Heilig, S., Ivanova, E., Kienast, M., Pelejero, C., Pflaumaan, U.: East Asian monsoon climate during the Late Pleistocene: high-resolution sediment records from the South China Sea, Mar. Geol., 156, 245–284, 1999.

Wang, Y., Cheng, H., Edwards, R. L., An, Z., Wu, J., Shen, C., and Dorale, J. A.: A high-resolution absolute-dated late Pleistocene monsoon record from Hulu Cave, China, Science, 294, 2345–2348, 2001.

Wang, Y., Cheng, H., Edwards, R. L., Kong, X., Shao, X., Chen, S., Wu, J., Jiang, X., Wang, X., and An, Z.: Millennial and orbital-scale changes in the East Asian monsoon over the past 224,000 years, Nature, 451, 1090–1093, 2008.

Xiao, J., Porter, S. C., An, Z., Kumai, H., and Yoshikawa, S.: Grain size of quartz as an indicator of winter monsoon strength on the Loess Plateau of central China during the last 130,000 yr, Quaternary Res., 43, 22–29, 1995.
Yancheva, G., Nowaczyk, N. R., Mingram, J., Dulski, P., Schettler, G., Negendank, J. F. W., Liu, J., Sigman, D. M., Peterson, L. C., Haug, G. H.: Influence of the intertropical convergence zone on the East Asian monsoon, Nature, 445, 74–77, 2006.
Yang, S. and Ding, Z.: A 249 kyr stack of eight loess grain size records from northern China documenting millennial-scale climate variability, Geochem. Geophy. Geosy., 15, 798–814, 2014.
Yang, Z., Lin, Z., and Yu, M.: Multi-scale analysis of East Asian winter monsoon evolution and Asian inland drying force (in Chinese), Quaternary Sci. Rev., 31, 73–80, 2011.
Yuan, D., Cheng, H., Edwards, R. L., Dykoski, C. A., Kelly, M. J., Zhang, M., Qing, J., Lin, Y., Wang, Y., Wu, J., Dorale, J. A., An, Z., and Cai, Y.: Timing, duration, and transitions of the last interglacial Asian monsoon, Science, 304, 575–578, 2004.
Zhang, R. and Delworth, T. L.: Simulated tropical response to a substantial weakening of the Atlantic thermohaline circulation, J. Climate, 18, 1853–1860, 2005.

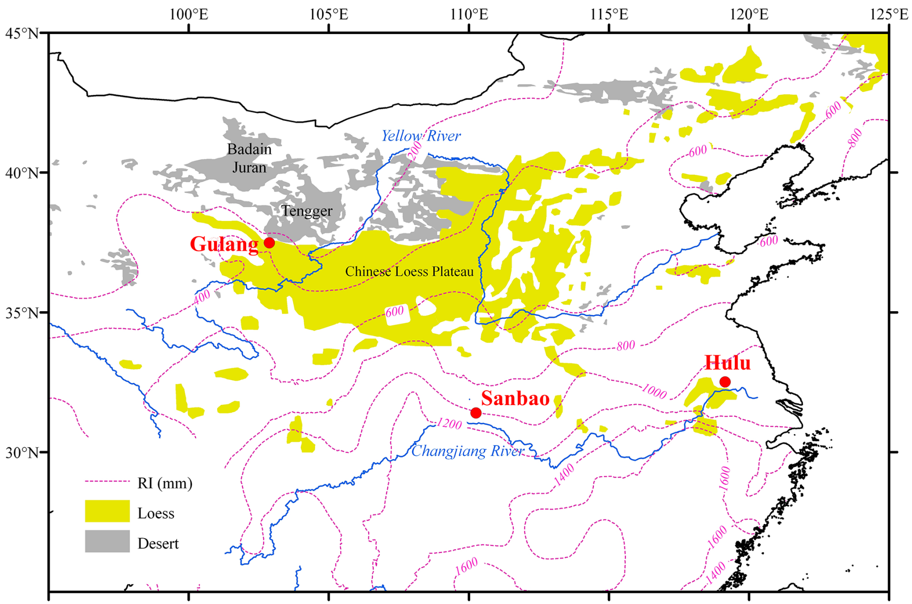

Figure 1. The locations of the loess sampling site at Gulang as well as Sanbao and Hulu caves.

CPD
10, 4623–4646, 2014

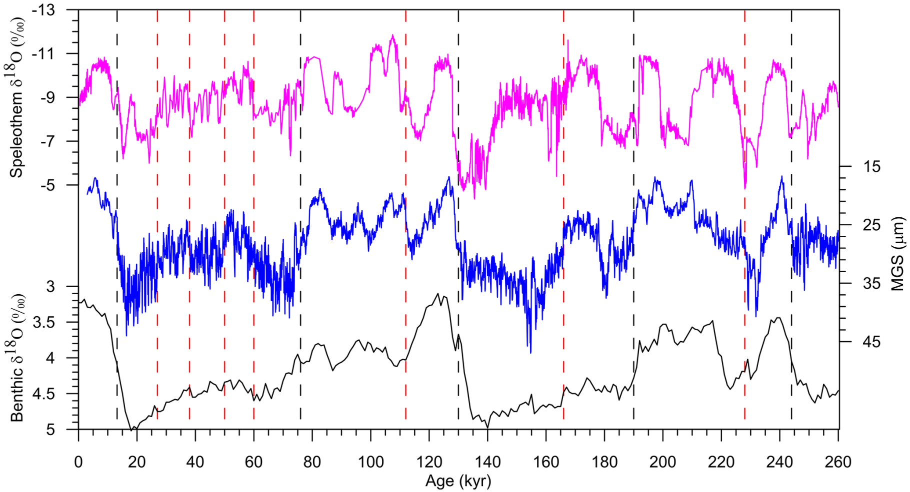

Figure 2. Comparison of Gulang MGS (blue) with the benthic $\delta^{18}O$ (black) (Lisiecki and Raymo, 2005) and Sanbao/Hulu speleothem $\delta^{18}O$ (purple) (Wang et al., 2008; Cheng et al., 2009) records. The black and red dashed lines denote tie points linking the MGS to abrupt changes in benthic $\delta^{18}O$ (Lisiecki and Raymo, 2005) and speleothem $\delta^{18}O$ records (Wang et al., 2008; Cheng et al., 2009), respectively.

CPD
10, 4623–4646, 2014

Multiscale monsoon variability during the last two climatic cycles

Y. Li et al.

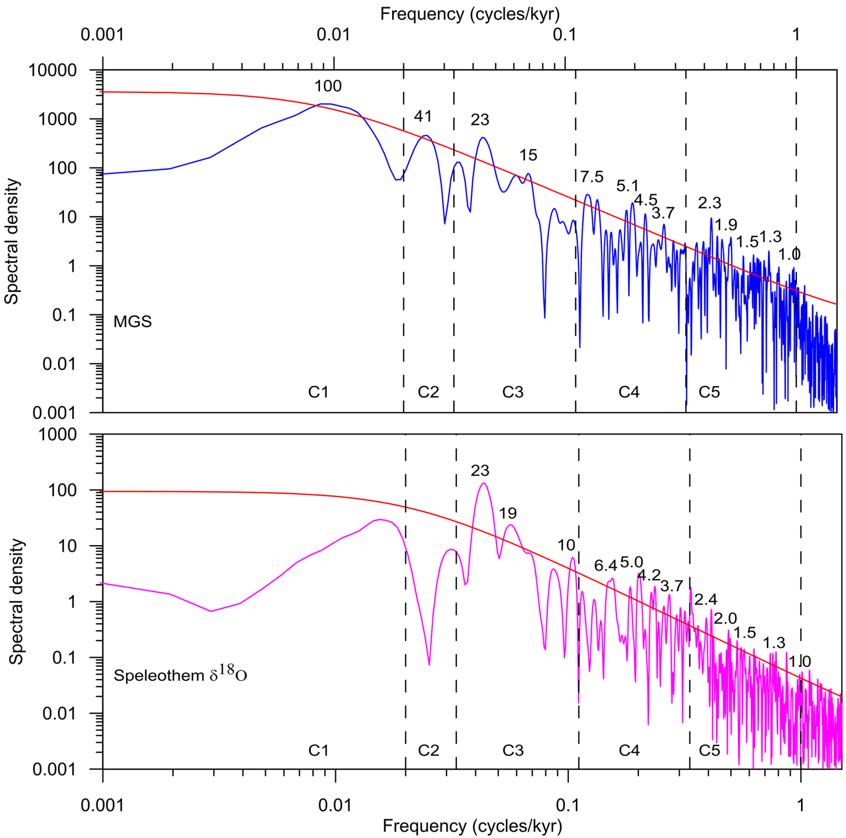

Figure 3. Spectrum results of Gulang MGS (blue) and Sanbao/Hulu speleothem δ^{18}O (purple) (Wang et al., 2008; Cheng et al., 2009) records. The red lines represent the 80 % confidence levels; the numbers in black are identified periods in kyr, and the dotted lines are boundaries for the six components decomposed from the initial records.

CPD
10, 4623–4646, 2014

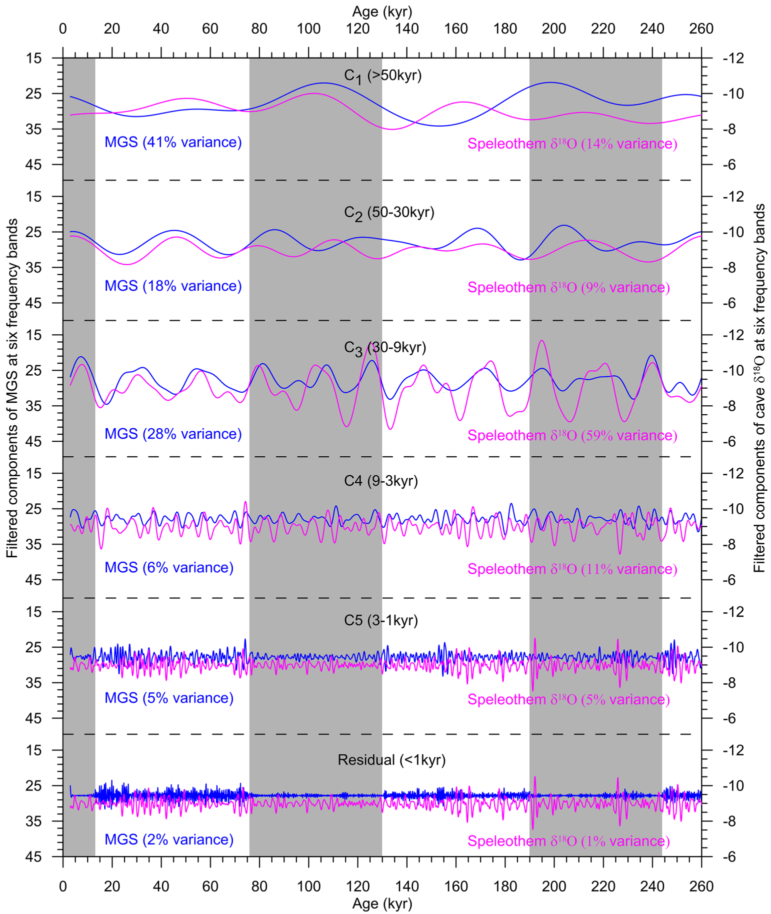

Figure 4. The filtered components of Gulang MGS (blue) and Sanbao/Hulu speleothem δ^{18}O (purple) (Wang et al., 2008; Cheng et al., 2009) records at six frequency bands. The vertical gray bars indicate the interglacial periods.

CPD
10, 4623–4646, 2014

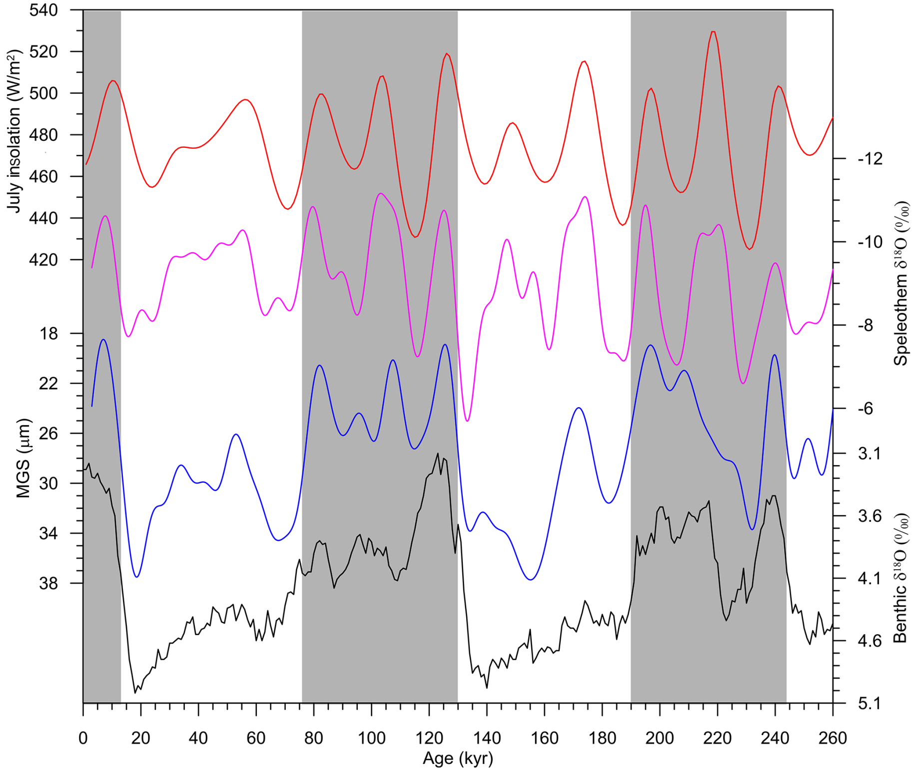

Figure 5. Comparison of the glacial- and orbital-scale components (filtered > 9 kyr) of Gulang MGS (blue) and Sanbao/Hulu speleothem $\delta^{18}O$ (purple) (Wang et al., 2008; Cheng et al., 2009) records with summer insolation at 65° N (red) (Berger, 1978) and benthic $\delta^{18}O$ record (black) (Lisiecki and Raymo, 2005). The vertical gray bars represent the interglacial periods.

CPD
10, 4623–4646, 2014

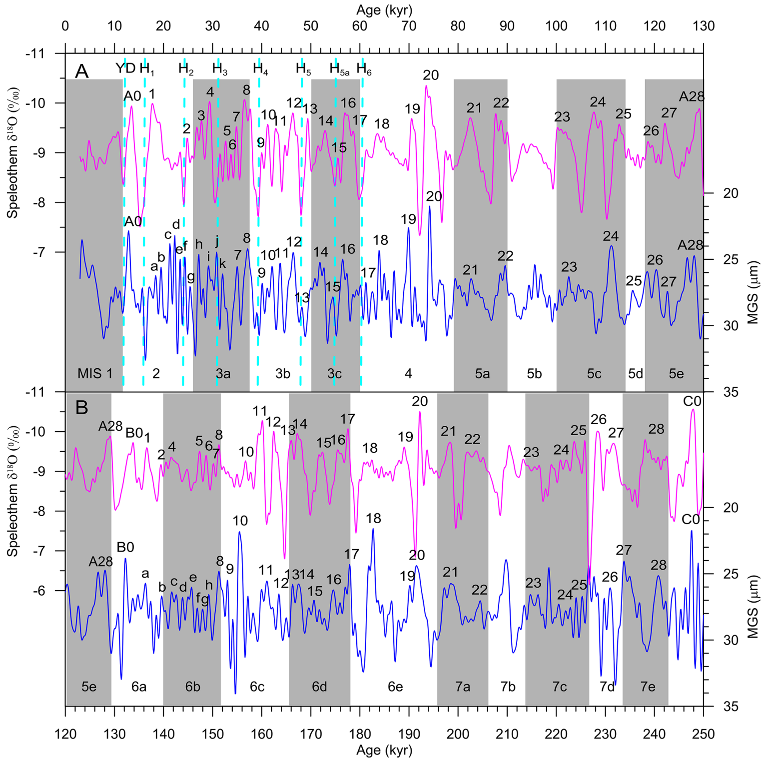

Figure 6. Comparison of millennial-scale (filtered 9–1 kyr) variations between Gulang MGS (blue) and Sanbao/Hulu speleothem $\delta^{18}O$ (purple) (Wang et al., 2008; Cheng et al., 2009) records over the last **(a)** and penultimate **(b)** glacial–interglacial cycles. Cyan and gray bars are, respectively, the Heinrich events recorded in the two records and interglacial periods. The letters denote distinct fluctuations in Gulang MGS signals which are not well aligned with speleothem record while the numbers (34–130 and 152–250 kyr) represent well-correlated Chinese interstadials identified in the two records.

CPD
10, 4623–4646, 2014